Experimental assessment of passive radiator parameters using normal-incidence sound transmission measurements



Brian E. Anderson ⁽ⁱ⁾; Spencer T. Neu; Joshua F. Gregg; Sarah M. Young; Timothy W. Leishman



J. Acoust. Soc. Am. 158, 3697-3710 (2025) https://doi.org/10.1121/10.0039708





Articles You May Be Interested In

Experimental extraction of loudspeaker parameters from sound transmission measurements in a plane wave tube for moving-coil drivers and passive radiators

J. Acoust. Soc. Am. (October 2019)

Evaluation of moving-coil loudspeaker and passive radiator parameters using normal-incidence sound transmission measurements: Theoretical developments

J. Acoust. Soc. Am. (July 2013)

Spider resonance frequency assessment using normal-incidence, transmission loss measurements

J. Acoust. Soc. Am. (April 2025)











Experimental assessment of passive radiator parameters using normal-incidence sound transmission measurements

Brian E. Anderson, ^{a)} Dependent T. Neu, Joshua F. Gregg, Sarah M. Young, and Timothy W. Leishman *Acoustics Research Group, Department of Physics and Astronomy, Brigham Young University, N283 Eyring Science Center, Provo, Utah 84602, USA*

ABSTRACT:

Passive radiators are notoriously difficult to characterize because one cannot effectively assess their mechanical parameters with loudspeaker electrical impedance techniques and no motors. This paper discusses the details of passive radiator and dynamic loudspeaker driver parameter measurements through practical experiments conducted with a plane wave tube, the two-microphone transfer function technique, and the two-load method to remove the need for an ideal anechoic termination. A previous theoretical paper demonstrated how normal-incidence transmission losses through these devices in an anechoically terminated tube could yield their mechanical and electrical parameters [Leishman and Anderson, J. Acoust. Soc. Am. **134**(1), 223–236 (2013)]. The mechanical parameters follow from an open-circuit transmission loss condition, whereas a driver's electrical parameters follow from an additional closed-circuit condition. This paper presents several experimental results and compares extracted parameters to those derived from electrical impedance measurements and destructive methods. In addition to other parameters, the masses of diaphragm assemblies show favorable agreement. The presented techniques effectively assess passive radiator parameters without employing active driver configurations and then removing their motors, which changes the measured properties. PACS numbers: 43.38.Ja, 43.20.Ye, 43.20.Mv, 43.55.Rg

© 2025 Acoustical Society of America. https://doi.org/10.1121/10.0039708

(Received 9 June 2025; revised 17 September 2025; accepted 9 October 2025; published online 7 November 2025)

[Editor: James F. Lynch] Pages: 3697–3710

NOMENCLATURE

- Bl Force factor, the product of the magnetic flux densityB in the magnet air gap and the effective length l of the voice-coil conductor in the magnet air gap
- Bl_n Estimated force factor from the nth curve-fitting iteration
 - c Speed of sound in air, \approx 343 m/s in Provo, UT at room temperature
- C_{MS} Mechanical compliance of the driver suspension
- $C_{MS,n}$ Estimated mechanical compliance of the driver suspension from the nth curve-fitting iteration
 - D Length of the downstream tube and distance between the measurement positions for R_B and R_C
 - *ê* Voltage
 - \hat{e}_R Voltage drop across the test resistor
 - f₀ In vacuo resonance frequency of the driver diaphragm and suspension system
 - f_l Lower-frequency limitation
 - f_s Free-air resonance frequency of the driver
 - f_u Upper-frequency limitation
 - H_{ab} Transfer function between the acoustic pressures at microphone positions a and b, $= \hat{p}_b/\hat{p}_a$
 - H'_{ab} Transfer function between the acoustic pressures at microphone positions a and b with a secondary downstream tube termination, $= \hat{p}'_b/\hat{p}'_a$

- $H_{\text{cal},ab}$ Relative calibration transfer function
- $H_{m,ab}^{o}$ Measured transfer functions between microphone signals for original positions
- $H_{m,ab}^{s}$ Measured transfer functions between microphone signals for switched positions
 - ê Electrical current
 - j Imaginary number, $=\sqrt{-1}$
 - k Lossless acoustic wavenumber
 - Complex acoustic wave number accounting for propagation losses in the plane wave tubes
 - L_n Distance from the *n*th microphone to the device under test (DUT)
 - L_E Effective electrical inductance of the driver voice coil
- $L_{E,n}$ Estimated effective electrical inductance of the driver voice coil from the nth curve-fitting iteration
- M_{MD} Effective mechanical mass of the driver diaphragm assembly without fluid loading
- $M_{MD,n}$ Estimated mechanical mass of the driver diaphragm assembly without fluid loading, from the nth curve-fitting iteration
- M_{MS} Effective mechanical mass of the driver diaphragm assembly with fluid loading
 - \hat{p}_n Complex acoustic pressure amplitude at the *n*th microphone position
 - R Test resistance
 - R_A Reflection coefficient looking into the DUT at the end of the upstream tube

a)Email: bea@byu.edu

https://doi.org/10.1121/10.0039708



- R'_A Reflection coefficient looking into the DUT at the end of the upstream tube with a secondary downstream tube termination
- R_B Reflection coefficient looking into the downstream tube past the DUT
- R_C Reflection coefficient of the downstream tube termination
- R'_{C} Reflection coefficient of a secondary downstream tube termination
- R_D Intermediate reflection coefficient defined for mathematical simplification of R_B
- R_E Direct current electrical resistance of the driver voice coil
- R_{MS} Mechanical resistance of the driver suspension
- $R_{MS,n}$ Estimated mechanical resistance of the driver suspension from the nth curve-fitting iteration
 - s Microphone spacing
 - S Cross-sectional area of the plane wave tube
 - S_D Effective cross-sectional area of the driver diaphragm (the convention of measuring the diameter of the cone plus half of the width of the surround on both sides of the cone is used here)
 - TL Transmission loss
 - X_E Blocked electrical reactance of the voice coil
- Z_{EB} Blocked electrical impedance of the voice coil
- $Z_{E,in}$ Input electrical impedance of the DUT
- Z_M Mechanical impedance of the diaphragm and suspension system
- Z_{MS} Mechanical impedance of the diaphragm and suspension system with fluid loading
- α_C Absorption coefficient of the downstream tube termination
- ho_0 Ambient density of air, $\approx 1.01 \, \mathrm{kg/m^3}$ in Provo, UT at room temperature
- τ Transmission coefficient
- au_{OC} Open-circuit transmission coefficient
- au_{CC} Closed-circuit transmission coefficient
 - ω Angular frequency

I. INTRODUCTION

The electrical and mechanical parameters that characterize the linear operation (small-signal regime) of movingcoil loudspeaker drivers typically follow from electrical excitation or measurement but may also result from acoustical methods.² Several techniques use electrical input impedance as a basis for parameter extraction. A common approach involves measuring the "free-air" input impedance and a second impedance following a known perturbation (e.g., an added mass to the cone or a closed-box loading to modify the suspension compliance). 1,3–19 To avoid the need for two electrical impedance measurements, some authors have suggested simultaneous measurements of electrical impedance and dynamic cone motion or acoustic pressure adjacent to the cone. 20-29 Others have developed optimization or curve-fitting techniques to extract parameters from a single free-air electrical impedance measurement. 30-36

Clark²² and Klippel²⁵ employed pneumatic pressure to shift the cone rest position and, thus, measure the parameters as a function of static displacement.

Unfortunately, none of the electrical techniques may directly measure the mechanical parameters of a passive radiator (also known as a drone cone or auxiliary bass radiator³⁷) because there is no coupling of mechanical and electrical impedances. For passive radiators manufactured as loudspeaker driver components with their magnet and voice-coil assemblies removed, ³⁷ approximate mechanical parameters are measurable with the motors intact. However, the motor removal alters their radiation loading effects. A standard existed to estimate passive radiator parameters through acoustic excitation (the setup did not employ a plane wave tube) and observation of the frequency of maximum displacement, ³⁸ but the publishing society later withdrew it. The work of Klippel, ²⁵ using pneumatic pressure, employed a similar setup to predict the parameters.

Because loudspeakers are electro-mechano-acoustical devices, their parameters should indeed follow from appropriate acoustical or mechanical measurements. Theoretical expressions for the transmission loss of one-dimensional sound through a driver or passive radiator allow the extraction of parameters from the measurement of the transmission loss using a plane wave tube. Two of the present authors (T.W.L. and B.E.A.) presented preliminary theoretical and experimental results confirming this assertion for loudspeaker drivers.³⁹ Their conference paper described experimental work using a very long plane wave tube with a square $(30.5 \text{ cm} \times 30.5 \text{ cm})$ cross section, a quasi-anechoic passive downstream termination, and a limited measurement bandwidth of approximately 70–500 Hz. The imperfect absorption of the 246 cm long termination likely skewed the measurement results, yielding extracted parameters differing by 20% or more from the parameters assessed via electrical impedance techniques. In a subsequent paper, these authors provided further theoretical insights into such measurements, including those associated with imperfect anechoic terminations, methods of parameter extractions, and the benefits of decomposing downstream sound fields into propagating components.²

This paper aims to provide experimental details demonstrating that one may assess the parameters of passive radiators and drivers from improved sound transmission measurements with comparable accuracy to those derived from electrical impedance assessments of drivers. The parameters follow from normal-incidence sound transmission loss coefficient measurements using the methods proposed in Ref. 2, along with parameters extracted from measurement curve fitting. Importantly, the two-load sound transmission measurement technique automatically corrects for nonideal termination conditions, improves results, and makes the measurements more practical as a long anechoic termination is unnecessary. The work demonstrates that one may assess passive radiators and changes made to them using sound transmission measurements, whereas evaluations via electrical impedance measurements are impractical. The approach does not replace electrical impedance techniques for drivers nor does it show whether sound transmission techniques can extract all parameters obtainable through electrical impedance techniques and more complicated driver models. Instead, it complements these tools for more complete insights and assessments.

Although the authors have previously proposed the possibility of acoustical extraction of mechanical passive radiator parameters, they have not previously assessed and presented them. The experiments presented herein evaluated four drivers of the same make and model and four passive radiators produced by removing their magnets. The modifications allowed comparisons of extracted mechanical parameters with and without the magnets. To the authors' knowledge, the effect has not received careful attention or publication elsewhere. Subsequent modifications to the masses and compliances of the passive radiator cone assemblies provided additional opportunities for experimental evaluations. In addition, the authors employed a precision scale to assess the mechanical masses of destructively removed cone assemblies and individual components from the passive radiators. This final step allowed further comparisons of the mass values extracted from the sound transmission and electrical impedance measurements.

Section II briefly discusses transmission loss measurements using a plane wave tube and the two-microphone transfer function technique. Details of this investigation's particular system follow with an explanation of curve-fitting techniques. Sections V and VI compare parameters from the proposed method and conventional electrical impedance techniques. They also compare mechanical driver parameters determined acoustically following magnet removal and demonstrate how accurately the proposed technique detects changes in moving mass and suspension compliance of the passive radiators. Further validations follow from comparing the moving mass results extracted from the transmission loss and electrical impedance measurements with the masses obtained through destructive means.

This paper employs linear models for the drivers and passive radiators because of the small-signal excitation used in the experiments. It also assumes a simplistic model for the blocked electrical impedance of the driver voice coil. The authors do not suggest that these models best represent all loudspeakers. However, they simplify the introduction of the experimental methods and extraction of parameters from different types of transmission loss data. Future work could incorporate nonlinear driver parameter models and more sophisticated voice-coil models.

II. TRANSMISSION LOSS MEASUREMENTS

A. Two-microphone transfer function technique

The two-microphone transfer function technique, presented by Chung and Blaser (C and B)^{41,42} and described by others, ^{43–47} allows measurements of normal-incidence reflection and transmission coefficients of material samples or acoustical devices between upstream and downstream plane wave tubes. An upstream pair of microphones enables

decomposition of the upstream sound field into incident and reflected pressure components. A downstream pair of microphones also allows decomposition of the downstream field into the pressure transmitted past the device under test (DUT) and any pressure reflected residually by a quasi-anechoic termination. These pressure components lead to the computation of reflection and absorption coefficients, acoustic impedance, and the sound transmission coefficient for the DUT.

A relative calibration transfer function $H_{\text{cal},ab}$ between two signals a and b of a microphone pair corrects for their amplitude and phase mismatches. The function follows from the switching calibration technique⁴¹ and the geometric mean such that

$$H_{\text{cal},ab} = \sqrt{H_{m,ab}^O H_{m,ab}^S},\tag{1}$$

where, as indicated in the Nomenclature, $H^o_{m,ab}$ and $H^s_{m,ab}$ represent the measured transfer functions between the microphone output signals in their original and switched positions, respectively. The transfer functions between the total acoustic pressures at the microphone positions follow as

$$H_{ab} = \frac{H_{m,ab}^O}{H_{\text{cal},ab}}. (2)$$

C and B showed that the complex reflection coefficients R and transmission coefficient τ follow readily from these transfer functions. Then, the transmission loss follows as

$$TL = 10\log_{10}\left(\frac{1}{\tau}\right). \tag{3}$$

Although the C and B formulation resulted from a decomposition of upstream and downstream fields into incident and reflected components, it does not fully address the critical requirement that the downstream tube must have an ideal anechoic termination. Leishman and Anderson (L and A) illustrated the problems resulting from imperfect anechoic terminations and found that whereas the *TL* from C and B may improve on those of other methods, it continues to suffer from erroneous fluctuations over typical measurement bandwidths.²

B. Improved transmission coefficient

Other authors have periodically summarized developments in plane wave tube measurements, including more recently. 48,49 One significant advance has involved the sequential use of two distinct downstream tube terminations in the so-called two-load method. 50-52 This scheme aims to overcome the problems associated with imperfect termination properties. Salissou and Panneton (S and P)⁵³ presented a technique using two terminations and wave decomposition (the basis for the theory by C and B). Their approach

https://doi.org/10.1121/10.0039708

JASA

incorporated the two-microphone and switching calibration techniques, resulting in the measured transmission coefficient

$$\tau_{SP} = H_{23} \left(1 - R_B R_C e^{j2kD} \right) \frac{e^{jkL_2} + R_A e^{-jkL_2}}{e^{-jkL_3} + R_C e^{jkL_3}},\tag{4}$$

where the descriptions of each constant and variable appear in the Nomenclature. Figure 1 depicts the microphone positions. The transfer function $H_{23} = \hat{p}_3/\hat{p}_2$ is that measured between the complex acoustic pressure amplitude \hat{p}_2 at microphone 2, just upstream of the DUT, and the complex pressure amplitude \hat{p}_3 at the microphone 3, just downstream of the device.

The upstream complex reflection coefficient R_A at the DUT follows from

$$R_A = \frac{H_{12} - e^{-jks}}{e^{jks} - H_{12}} e^{j2k(s+L_2)},\tag{5}$$

where $H_{12} = \hat{p}_2/\hat{p}_1$ is the transfer function between the complex acoustic pressures at microphones 1 and 2. Here, the factor $e^{j2k(s+L_2)}$ propagates the coefficient from microphone 1 to the DUT, a distance of $s+L_2$. The downstream tube termination reflection coefficient R_C has a similar form

$$R_C = \frac{H_{34} - e^{-jks}}{e^{jks} - H_{34}} e^{j2k(D - L_3)},$$
(6)

where $e^{j2k(D-L_3)}$ propagates the coefficient from microphone 3 to the beginning of the termination. The reflection coefficient looking into the downstream tube just beyond the DUT is

$$R_B = \frac{R_D - \frac{H_{23}}{H'_{23}}}{R_D R'_C - \frac{H_{23}}{H'_{23}} R_C} e^{-j2kD},\tag{7}$$

where

$$R_D = \frac{e^{-jkL_3} + R_C e^{jkL_3}}{e^{-jkL_3} + R'_C e^{jkL_3}} \frac{e^{jkL_2} + R'_A e^{-jkL_2}}{e^{jkL_2} + R_A e^{-jkL_2}}.$$
 (8)

This result employs reflection coefficients and transfer functions assessed with the two distinct termination loads. Unprimed variables are those involving the first load (a quasi-anechoic downstream termination for this study). Primed variables are those involving the second load (an open downstream tube for this study). The factor e^{-j2kD} involves a negative exponent, which propagates the reflection coefficient upstream from the termination to the transmitting side of the DUT.

The insertions of the various reflection coefficients into Eq. (4) yield τ_{SP} and then TL_{SP} from Eq. (3). A complex wavenumber \tilde{k} in the formulations addresses thermo-viscous tube losses, which is derived from an estimated attenuation coefficient based on a published coefficient of shear

viscosity, a ratio of specific heats, and a Prandtl number in air at $20\,^{\circ}\text{C}$. Realistically, the small attenuation effects are nearly negligible over the measurement distances for these "wide tubes," but their inclusion helps improve the accuracy of the calculations.

III. PLANE WAVE TUBE SYSTEM

A. Measurement bandwidth

Figure 1(a) shows a photograph of the plane wave tube measurement system used in the experiments, and Fig. 1(b) illustrates the system diagrammatically. The DUT, a driver or passive radiator mounted to a rigid circular baffle, separated the upstream and downstream tubes (see Fig. 3). Microphones 1 and 2 were the upstream pair with either a low-frequency or high-frequency spacing, whereas microphones 3 and 4 were the downstream pair with a similar spacing. The upstream and downstream tubes had 10.2 cm (4 in.) inside diameters and 1.5 m lengths, meaning that the cutoff frequencies of their first cross modes were approximately 1970 Hz (i.e., only plane waves propagated below this frequency at room temperature [20 °C]).⁵⁵ Notably, the proposed measurement method scales such that larger or smaller tube diameters allow piston-band measurements of larger or smaller DUTs, respectively.

The downstream tube termination consisted of a tapered wedge of open-cell foam rubber, a backing gap filled with loose polyester fiberfill, and a rigid steel cap. Sagers *et al.*⁵⁶ used this same equipment and found that its anechoic cutoff frequency was approximately 67 Hz. This meant that for frequencies below 67 Hz, the reflection coefficient was $|R_C| > 0.1$ and the absorption coefficient was $\alpha_C = 1 - |R_C|^2 < 0.99$. The plane wave tube, thus, provided a usable bandwidth of approximately 67–1970Hz for normal-incidence sound transmission measurements.

The extraction of several parameters listed in the Nomenclature required TL measurements through the DUT below, near, and above its resonance frequency. For an open-circuit DUT, the suspension system's compliance C_{MS} dominated TL well below resonance. Well above resonance, the *in vacuo* moving mass M_{MD} of the diaphragm assembly dominated TL. Near resonance, the mechanical reactance resulting from C_{MS} and M_{MD} vanished, leaving the viscous mechanical resistance R_{MS} of the DUT suspension to govern TL.

For the purposes of this investigation, the experiments specifically evaluated four Tang Band model W3-881SJ drivers (Taipei, Taiwan) with nominal 3 in. (7.6 cm) diameters and roughly 100 Hz free-air resonance frequencies. The effective radiating areas of these drivers, determined using the convention of measuring the diameter of the cone plus half of the surround width on either side of the cone, were $S_D = 30.76 \, \text{cm}^2$. It is noteworthy that the IEC 60268-22 standard presents conflicting descriptions of how to calculate S_D .⁵⁷ Section 20.8.2.4 of IEC 60268-22 initially suggests that one should add half the surround *area* to the cone area in the calculation but later presents an equation

JASA https://doi.org/10.1121/10.0039708

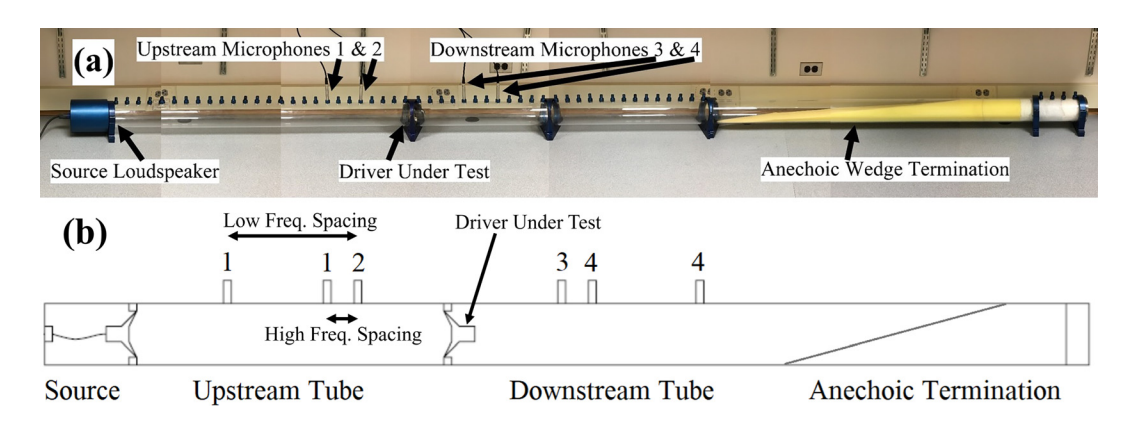


FIG. 1. (a) Photograph of the plane wave tube system employed for the measurements of this work is displayed. Several photographs stitched together formed this image. The microphones in the photo were not placed at the exact measurement locations. (b) Diagram of the same plane wave tube system (not to scale) is shown. Note the two spacings for the upstream and downstream microphone pairs used to measure, respectively, low-frequency and high-frequency reflection coefficients accurately.

[Eq. (14)], assuming that S_D derives from the convention we use here. The two definitions do not strictly agree because the latter includes less than half the total surround area in S_D . Another S_D calculation represents the surround's displacement amplitude as tapering linearly from its inner perimeter to zero at its outer perimeter, suggesting that the air volume displaced by a circular diaphragm assembly corresponds to that within a right circular conical frustum. ^{56,58,59} The resulting effective radiating area converges to the S_D of this work when the surround width becomes much smaller than the cone radius. ⁵⁹

The ASTM E1050-24 and E2611-24 standards regulate the use of plane wave tubes for testing the acoustical properties of material specimens. Both require the closest microphone positions to fall at least three tube diameters from an excitation source, one tube diameter from a rough nonhomogenous specimen, and two tube diameters away from a rough asymmetric specimen to suppress cross-mode field contributions adequately. For this work, the microphones fell at least 0.5 m (five tube diameters) away from any tube boundary for the upstream and downstream tubes.

Bodén and Åbom⁶² proposed microphone spacing limits to ensure less than 1% error for measurements via the two-microphone transfer function technique. Their expression $0.1\pi < ks < 0.8\pi$ results in lower and upper-frequency limitations, respectively, for a given spacing s such that

$$f_l = \frac{c}{20s},\tag{9}$$

$$f_u = \frac{2c}{5s}. (10)$$

The chosen center-to-center microphone spacings of 30 and 5 cm provided bandwidths of 57–457 and 343–2744 Hz, respectively, allowing spectral overlap between 343 and 457 Hz. A crossover frequency of 400 Hz produced a transition for the measured data. More details about design considerations for plane wave tubes are available in standards 43,46,60 and other papers. 63,64

B. Measurement details

A Brüel and Kjaer Pulse measurement system (HBK, Darmstadt, Germany) generated a linear sine sweep excitation signal spanning 1-2000 Hz at a rate of 150 Hz/s to drive the source loudspeaker via a power amplifier. The system simultaneously acquired the responding microphone signals. The fast Fourier transform (FFT) measurement mode used 6400 lines spanning a 2 kHz bandwidth with 25 averages and 25% overlap. Sound pressure levels (SPLs) measured at microphones 2 and 3 gave a sense of the acoustic amplitudes used in the experiments. Figure 2(a) provides typical plots of the levels over frequency. It is worth noting that these levels are not high enough to induce nonlinear acoustic effects but are high enough to exceed the noise floor of the measurement system by typically 40–50 dB. Figure 2(b) shows the typical coherence between the associated signals measured upstream and downstream, revealing values greater than 0.975 for the measurement bandwidth and 0.99 for all but three distinct frequencies, at which microphone 2 fell at a node. This high coherence illustrates that the downstream pressure resulted from the upstream pressure and not background noise. The typical uncertainty of the transmission loss measurements, determined from an average of the standard deviation values (deviations among the individual averages) between 67 Hz (anechoic limit) and 675 Hz (upper limit of curve fitting) was ± 0.07 dB.

Figure 3 displays photographs of a DUT mounted at the end of the upstream tube. Figure 3(a) shows it fastened to the steel aperture plate. The visible groove in the plate surrounding the driver frame accommodates an *O*-ring, which provides a tight seal with the adjoining downstream tube. Figure 3(b) depicts the back side of the driver through the transparent upstream tube. A wire connected its input terminals for closed-circuit measurements. In both photographs, one can observe the compression fitting involving a Klein Flansche flange arrangement. One may also note several pegs along the top of the upstream tube. Each is a removable, solid 1.27 cm diameter aluminum plug placed firmly within a microphone port with *O*-ring seals, which is nominally flush with the inner tube wall at one end. It is removable for

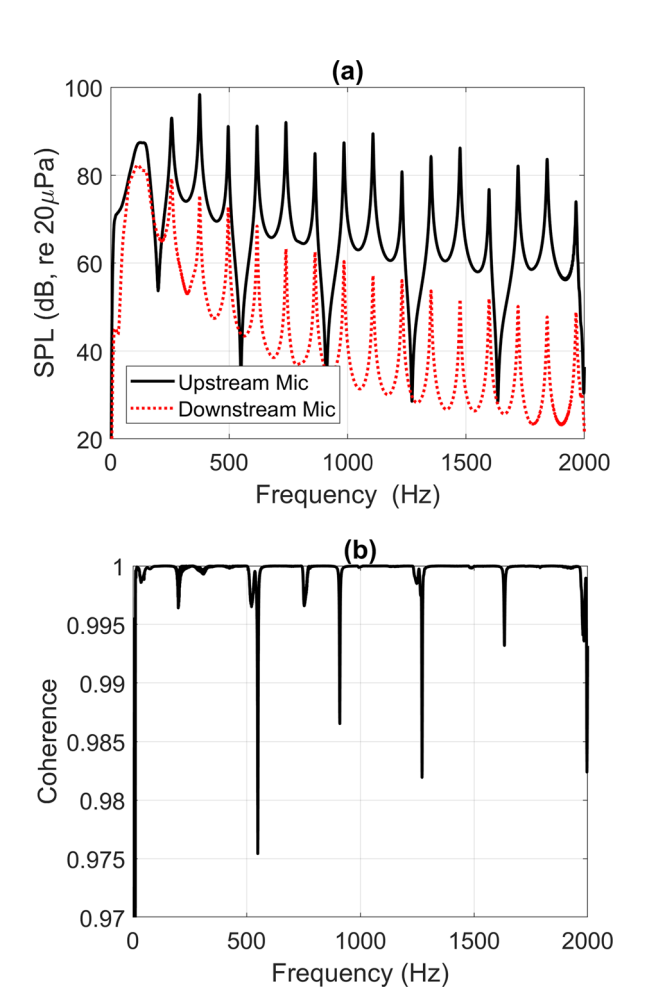


FIG. 2. (a) Sample SPL measurements at an upstream microphone (microphone 2) and a downstream microphone (microphone 3) during a sound transmission measurement and (b) sample coherence measurement between the upstream and downstream microphone signals are shown. The measurements involved the low-frequency spacings.

replacement with a microphone of the same diameter as needed. The center-to-center port spacing is 5.0 cm.

As suggested earlier, the two downstream tube terminations included the anechoic wedge depicted in Fig. 1 and an opening to the surrounding air. Experimentation with different load conditions determined that these two terminations worked well for the two-load method, meaning that they yielded data that matched theoretical curves for transmission through a damped, mass-spring system well. For example, it seemed that using a rigid cap end and an open end did not provide data that matched expected theory well, likely, because the two loads provide exactly opposite boundary conditions (same magnitude response but opposite phase), whereas it seems that two loads that provide different magnitudes and phases (such as an open end and an anechoic end) provide data that matches the expected theory better.

IV. PARAMETER EXTRACTION FROM SOUND TRANSMISSION

A. Theory

L and A derived an analytical expression for the opencircuit transmission coefficient τ_{OC} of a classically modeled,

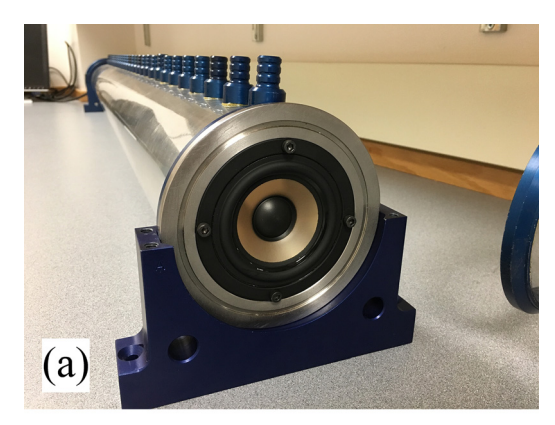




FIG. 3. (a) Photograph of a driver mounted to a partition at the end of the upstream tube and (b) photograph of the back side of the mounted driver through the transparent tube are shown.

rectilinearly vibrating, baffled DUT between an upstream tube and an anechoically terminated downstream tube [Ref. 2, Eq. (20)]. The sound transmission through the device compares the upstream volume velocity and impedance to the downstream volume velocity and acoustic impedance loading [Ref. 2, Eq. (11)]. The upstream impedance includes the device's internal impedance and downstream loading. L and A gave the reciprocal of $\tau_{\rm OC}$ for an arbitrarily terminated downstream tube [Ref. 2, Eq. (16)], which reduces to

$$\frac{1}{\tau_{\rm OC}} = \left| 1 + \frac{Z_M \left(\frac{S}{S_D} \right)^2}{2\rho_0 cS} \right| \tag{11}$$

when the downstream termination is anechoic, where

$$Z_M = R_{MS} + j\omega M_{MD} + \frac{1}{j\omega C_{MS}}. (12)$$

The commonly specified mass M_{MS} assumes equal front-and-back fluid mass loading that roughly approaches the loading of a transversely oscillating disk in free air⁵⁵ such that

$$M_{MS} \approx M_{MD} + \frac{8}{3}\rho_0 \left(\frac{S_D}{\pi}\right)^{1.5}$$
 (13)

The *in vacuo* resonance frequency f_0 associated with Z_M occurs when the reactance caused by the moving mass M_{MD} and compliance C_{MS} vanishes, whereas the free-air resonance frequency f_S includes the fluid mass loading, which inherently incorporates less understood backward radiation through and around the spider, voice-coil former, frame, and magnet structure (when present).

L and A also derived an expression for the closed-circuit (short-circuit) transmission coefficient τ_{CC} through a driver with an arbitrary downstream tube termination [Ref. 2, Eq. (17)]. The closed-circuit condition assumes a wire of zero electrical impedance connecting the driver terminals. If the downstream tube termination is anechoic, the reciprocal expression reduces to

$$\frac{1}{\tau_{\rm CC}} = \left| 1 + \frac{Z_M + \frac{(Bl)^2}{Z_{EB}}}{2\rho_0 cS} \left(\frac{S}{S_D} \right)^2 \right|^2,\tag{14}$$

where

$$Z_{EB} \approx R_E + j\omega L_E$$
 (15)

is an approximate blocked electrical impedance of the voice coil, R_E is the voice-coil resistance (measured with a multimeter), and L_E is the voice-coil inductance. As noted previously, a more sophisticated Z_{EB} model could also represent the impedance.⁶⁵

B. Transmission loss measurement and parameter extraction

Figures 4(a) and 4(b) show example *TL* curves for open- and closed-circuit conditions using the methods by C and B) and S and P [based on Eq. (4)]. The C and B *TL*s includes erroneous fluctuations, mostly below 400 Hz, as described by L and A, whereas the S and P *TL*s compare well with theoretical curves (e.g., Fig. 8 of Ref. 2) and the curve fits of Figs. 4(c) and 4(d), which assume an anechoic termination.

For the open-circuit case, the mass-spring resonance, occurring just above 100 Hz, yields the minimum TL governed by the suspension system's mechanical resistance R_{MS} . By assuming that the termination is anechoic, one may obtain R_{MS} [see Eq. (28) of L and A^2] With decreasing frequency below resonance, the increasing impedance of the suspension compliance C_{MS} governs the TL slope, and one may obtain C_{MS} using Eq. (32) of Ref. 2. Above resonance, the increasing impedance of the moving cone assembly mass M_{MD} governs the slope, and one may obtain M_{MD} using Eq. (33) of Ref. 2. An estimate of M_{MS} then follows from M_{MD} using Eq. (13).

The reason for the TL discrepancy in the 800–1000 Hz region is uncertain, although it may result from an independent resonance of the suspension system. The sharp rise in TL above 1800 Hz is a result of the increasing influence of the first tube cross mode. The minor disruption near 400 Hz

is likely caused by slight differences in the measured TL s by the low- and high-frequency microphone spacings. The increased TL near the resonance frequency for the closed-circuit condition is due to the back electromotive force from the induced voice-coil current as it moves within the magnetic field. One may extract the Bl and L_E values from the closed-circuit TL using Eqs. (37) and (42) from Ref. 2, respectively.

As noted previously, L and A² and Anderson and Leishman³⁹ gave several expressions to extract loudspeaker parameters from measured TL s. They are complicated and require the selection of valid \pm roots to keep the results real. Furthermore, the expressions for C_{MS} , M_{MD} , and Bl are asymptotic and valid only in high- or low-frequency limits, which may fall outside of the bandwidth of a given measurement system and driver. The average R_{MS} , C_{MS} , M_{MS} , Bl, and L_E parameters extracted from the C and B and S and P TL techniques, using the L and A expressions, appear in Table I (note that parameters derived from curve fitting of electrical impedance measurements will be described in Sec. V). Notably, the C_{MS} and Bl values differ most, depending on the use of the C and B or S and P techniques. This is because the extraction of these parameters depends most strongly on the accuracy of the low-frequency TL, where the wedge may not provide an ideal anechoic loading as required for good C and B results. The L and A expression used to extract the C_{MS} value relies on an asymptotic approximation valid for low frequencies far from the resonance frequency, which may not be the case for this data set with a resonance frequency of only $\sim 100\,\mathrm{Hz}$. This issue illustrates the benefit of using the two-load S and P TL for parameter extractions.

C. Curve fitting and parameter extraction

Table I also includes parameters extracted from the openand closed-circuit sound transmission measurements using a curve-fitting algorithm implemented in MATLAB (The MathWorks, Natick, MA). The algorithm used the fminsearch. m function from MATLAB, employing the Nelder-Mead simplex direct search method of Lagarias et al. 66 The curve fitting idealized the measurements as involving anechoic terminations (a reasonable assumption for the S and P technique in particular), meaning Eqs. (11) and (14) were the analytical bases. The algorithm employed the driver manufacturer's published parameters as initial values and subsequently yielded parameters that best fit the data. Several curve-fitting rounds confirmed the best possible estimations, where individual mechanical parameters dominate the transmission loss in specific frequency ranges. The additional rounds did not substantially increase the processing time.

For the open-circuit sound transmission measurements, a first round of fitting produced $R_{MS,1}$, $M_{MD,1}$, and $C_{MS,1}$, which were closer to the values obtained with the S and P TL final curve fit and values extracted from electrical impedance than the initial published values. (Detailed analysis of the accuracy of the initial values and their impacts on

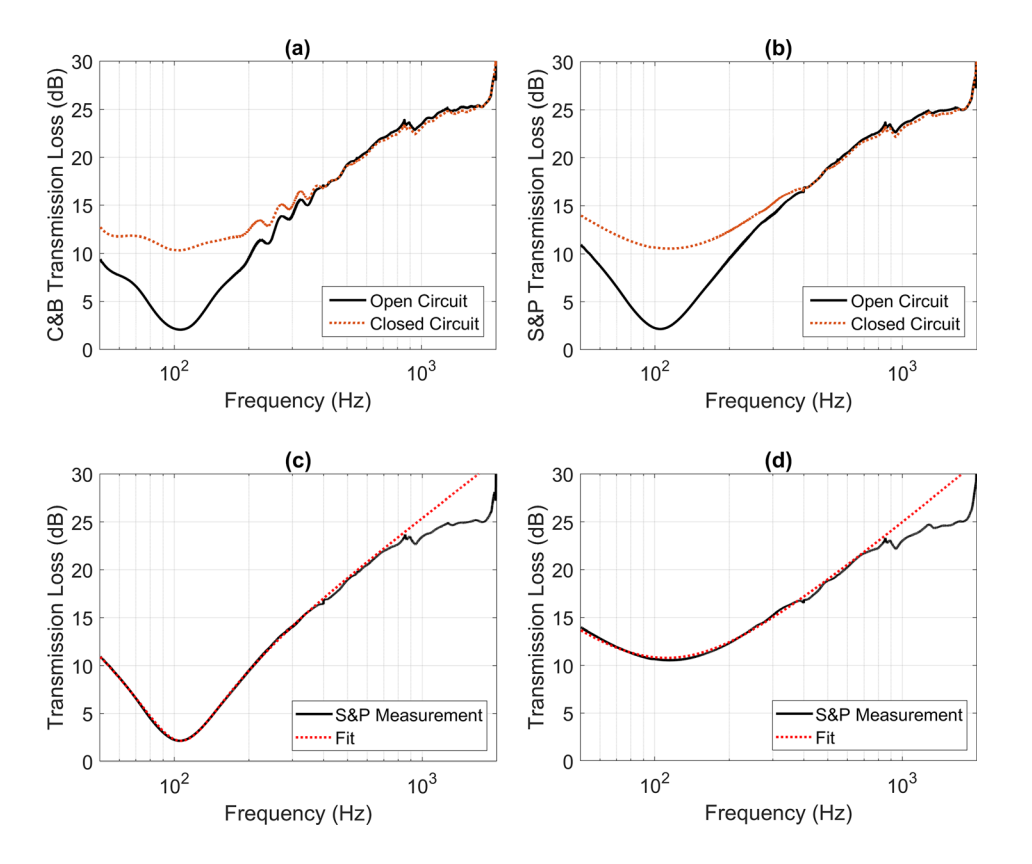


FIG. 4. (a) Open and closed-circuit TL measurements using the C and B technique, (b) open- and closed-circuit TL measurements using the S and P technique, (c) open-circuit TL measurement of a driver using the S and P technique and a curve fit to the data, and (d) closed-circuit TL measurement of a driver using the S and P technique and a curve fit to the data are shown.

extracted results is beyond the scope of this work, but the curve fitting does not appear to be very sensitive to the initial values used.) For the first curve-fitting round, the bandwidth was 1-675 Hz to avoid the previously mentioned 800–1000 Hz disparity. A second round of fitting employed the $M_{MD,1}$ and $C_{MS,1}$ values from the first round as fixed values and then optimized $R_{MS,2}$ as the final R_{MS} estimate. In this case, the bandwidth was 80.6–134.7 Hz (the approximate resistance-controlled region), corresponding to the span over which $TL < 4 \, dB$. For the third round of fitting, $R_{MS,2}$ and $C_{MS,1}$ were fixed values, and the routine optimized $M_{MD,3}$ was the final M_{MD} estimate, with the bandwidth limited to 134.7-362.5 Hz (the mass-controlled region). The fourth and final round of curve fitting employed $R_{MS,2}$ and $M_{MD,3}$ as fixed values and optimized $C_{MS,4}$ as the final C_{MS} estimate, with the bandwidth 1-80.6 Hz (the compliancecontrolled region).

Figure 4(c) shows the fitted transmission loss based on Eq. (11) with the extracted $R_{MS,2}$, $M_{MD,3}$, and $C_{MS,4}$. The

agreement between the measured data and fit is within 1 dB up to 896 Hz. Over the bandwidth used in the curve fitting (1–362.5 Hz), the agreement is within 0.2 dB. Similar fits to data from the C and B measurements did not match quite as well because of the TL fluctuations resulting from an imperfect anechoic termination. The agreement between the measured C and B data and the corresponding fit was also within 1 dB up to 896 Hz, but fluctuations of up to 1 dB persisted throughout the bandwidth used in the curve fitting $(1-362.5 \,\mathrm{Hz})$. Equation (13) produced M_{MS} from M_{MD} and S_D . Table I reports the average parameters extracted from the four drivers' TL measurements for the initial curvefitting round ("first curve fit") and the final round ("final curve fit") using only the S and P data. The initial curvefitting round produced mechanical parameters within 5% of the final curve-fitting values and may have provided sufficient accuracy in some cases.

Open-circuit sound transmission is useful because the mechanical portion of a loudspeaker driver separates from

TABLE I. Loudspeaker parameters extracted from drivers and passive radiators using electrical impedance and sound transmission measurements. The values shown reflect the average values extracted from four drivers of the same model along with standard deviations.

	Electrical impedance added mass	Electrical impedance free-air curve fit	C and B TL L and A methods	S and P TL L and A methods	S and P TL first curve fit	S and P TL final curve fit	Passive radiator (PR), S and P TL final curve fit	Holey PR, S and P TL final curve fit
L_E (mH)	0.52 ± 0.013	0.52 ± 0.015	0.50 ± 0.28	0.52 ± 0.22	0.62 ± 0.14	0.61 ± 0.13	_	_
$Bl(T^*m)$	3.33 ± 0.15	3.44 ± 0.20	3.16 ± 0.13	3.44 ± 0.15	3.33 ± 0.097	3.29 ± 0.095	_	_
R_{MS} (kg/s)	0.20 ± 0.015	0.20 ± 0.022	0.20 ± 0.0098	0.21 ± 0.011	0.22 ± 0.0095	0.21 ± 0.012	0.21 ± 0.0080	0.20
$M_{MS}(g)$	2.32 ± 0.20	2.34 ± 0.27	2.35 ± 0.040	2.32 ± 0.039	2.41 ± 0.039	2.48 ± 0.027	2.53 ± 0.027	2.50
C_{MS} (μ m/N)	1100 ± 74	1090 ± 100	1650 ± 120	1300 ± 85	1000 ± 59	984 ± 53	1060 ± 86	1280

the electrical portion. The extracted parameters are, thus, uncontaminated by an incorrect Bl estimate or position-dependent value, 22 as can result from electrical impedance measurements. Additionally, the same measurement procedure yields a straightforward assessment of passive radiator parameters, which cannot be performed with electrical impedance measurements.

Another round of curve fitting on the closed-circuit transmission loss measurements employed $R_{MS,2}$, $M_{MD,3}$, and $C_{MS,4}$ as fixed values, plus a fixed value of R_E that was measured with a multimeter to obtain optimized values for Bl_5 and $L_{E,5}$ over a 1–675 Hz bandwidth. Figure 4(d) shows the measured closed-circuit TL using the S and P technique along with the curve-fitted TL based on Eq. (14) and the parameters R_E , $R_{MS,2}$, $M_{MD,3}$, $C_{MS,4}$, Bl_5 , and $L_{E,5}$. The agreement between the data and fit is, again, within 1 dB up to 896 Hz. Over the 1–362.5 Hz bandwidth used for the open-circuit curve fitting, the agreement is within 0.3 dB.

It is worth noting that Anderson⁶⁷ found that there are limitations on the size of the driver that may be assessed using plane wave tube measurements. Various sized drivers were studied, and when the surface area of the driver was less than one-seventh of the tube cross-sectional area, the extracted parameters were not reasonably estimated. The $(S/S_D)^2$ term in Eq. (14) helps to correct for smaller surface area drivers, but there were still apparent limitations. For the loudspeakers used here, $S_D = 30.76 \text{ cm}^2$, whereas the tube's $S = 81.07 \text{ cm}^2$ and, thus, $S_D/S = 1/2.6$, which is well within the 1/7 guideline that Anderson gave.

D. Passive radiators

Following the driver measurements, the drivers were converted (via magnet removals) into passive radiators with similar mechanical properties [see Fig. 5(a)]. Table I reports the average parameters of the four drivers and their passiveradiator (PR) counterparts, as extracted from the S and P TL measurements. One should not necessarily expect a passive radiator's mechanical parameters to exactly equal those of the associated driver as the magnet structure no longer impedes the sound inside and outside the coil former. Table I reveals that the average C_{MS} value increased by 7.6% for the passive radiators. This result seems reasonable because an intact driver's coil former cavity and magnet air gap likely increase the effective stiffness of the diaphragm assembly and, thus, lower the driver's measured C_{MS} . The average M_{MS} value is 2.2% higher for the passive radiator, and the average R_{MS} value is nearly identical. For clarity, note that these comparisons are made between the S and P TL final curve fit results for the drivers and PR, S and P TL final curve fit results for the passive radiators.

Additional *TL* measurements followed the sequential affixing of known masses of duct seal putty to one of the passive radiator cones. The masses ranged from 0.25 g to 2.50 g in 0.25 g increments, as determined by a precision scale. After their removal, follow-up assessments of the putty samples verified that their masses had not changed.

The overlaid transmission loss curves in Fig. 6(a), one for each added mass, make several things apparent. The resonance frequency consistently shifts downward with increasing mass, which causes the TL curves to progressively shift to the left (with higher TL at any given frequency that is at or above resonance frequency, indicated by the red arrow). The increase at higher frequencies is logical from inspection of Eqs. (11) and (12), as the $j\omega M_{MD}$ term dominates Eq. (12). At lower frequencies, $j\omega M_{MD}$ becomes insignificant compared to $1/j\omega C_{MS}$, which leads the curves in Fig. 6(a) to differ by smaller amounts and approach convergence at lower frequencies. Based on these measurements, the extracted changes in M_{MD} resulting from the added masses are all within 0.05 g of the actual added masses as determined by the precision scale. Some extracted values were slightly more than the added mass, whereas others were slightly less than the added mass. The average absolute value of percent errors across all added masses was 1.4%.

For this study, the authors cut four 0.63 cm diameter circular holes in a passive radiator spider at symmetric positions. Figure 6(b) shows the change in transmission loss without and with the holes. In the latter case, the resonance frequency shifted downward by approximately 2 Hz, and the transmission loss below resonance decreased. As expected, both of these effects occurred because of increasing C_{MS} . Table I reports the parameters extracted for the passive radiator without and with (holey PR) the spider perforations, showing that C_{MS} increased by 7.7%, M_{MS} decreased by



FIG. 5. (a) Photograph of an intact driver along with a driver of the same model with the magnet removed to produce a passive radiator and (b) photograph of the various pieces of the passive radiator after a destructive analysis had been performed to measure the masses of each moving component are shown.

1.6%, and R_{MS} decreased by 4.8% with the holes. The slight transmission loss increase above the original resonance frequency is caused by the downward shift in resonance frequency [compare Fig. 6(a)] and the mass-controlled region's earlier spectral onset. The effect results from a more significant increase in C_{MS} than decrease in M_{MD} from the spider's material removal.

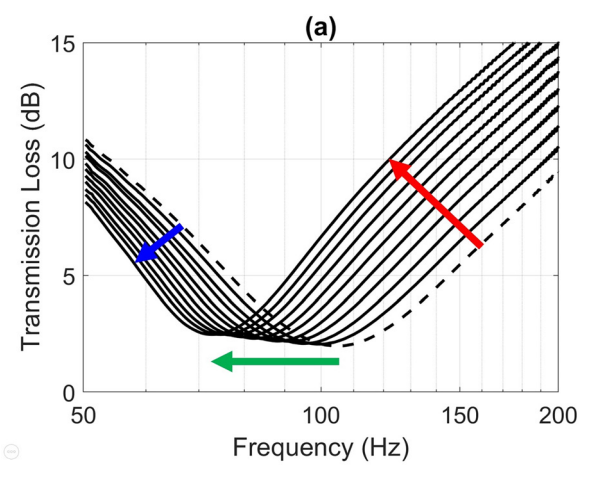
V. PARAMETER EXTRACTION FROM ELECTRICAL INPUT IMPEDANCE

Some loudspeaker driver parameters in Table I followed from electrical input impedance measurements to compare the results with the parameters obtained from the plane wave tube measurements. The same Brüel and Kjaer Pulse measurement system and frequency sweep settings produced the electrical measurements. The complex voltage amplitude \hat{e} across the driver terminals divided by the complex current amplitude \hat{i} through the voice coil equaled the DUT input impedance $Z_{E,in}$. A 7.07 V_{rms} amplitude chirp signal excited the driver in series with a $R = 998 \Omega$ resistance, thus, producing a peak current of about 10 mA, which was nearly constant over the 2 kHz bandwidth and small enough to ensure a small-signal measurement. The voltage drop across the resistor was $\hat{e}_R = iR$, such that $Z_{E,\text{in}} = R\hat{e}/\hat{e}_R$, where \hat{e}/\hat{e}_R was a measured complex transfer function. The \hat{e}_R measurement required floating the associated channel (i.e., its negative side was not grounded or shared with the other channel). An anechoic chamber provided a quiet free-field environment for the tests to isolate the drivers from the potential contamination of undesirable background noise and nonideal radiation conditions. The driver axes were held in the same horizontal orientation as in the plane wave tube. Using a linear operation model and a simplified voice-coil model, the free-air electrical impedance should theoretically follow from Eqs. (12), (13), and (15) as

$$Z_{E,\text{Driver}} = R_E + j\omega L_E + \frac{(Bl)^2}{R_{MS} + j\omega M_{MS} + \frac{1}{j\omega C_{MS}}}.$$
 (16)

The typical uncertainty of the electrical impedance magnitude measurements, determined from an average of the standard deviation values (deviations among the individual averages) between 67 and 675 Hz (same frequency range evaluated for transmission loss) was $\pm 0.03\,\Omega.$

A curve fit using Eq. (16) and the fminsearch.m function from MATLAB produced the parameters from the electrical impedance measurement, with the resistance R_E , again, resulting from a multimeter measurement. Curve fitting that used the manufacturer's published parameters as initial values produced the estimates $L_{E,1}$, Bl_1 , $R_{MS,1}$, $M_{MS,1}$, and $C_{MS,1}$. A second fitting employed the $L_{E,1}$ value from the first round to obtain Bl_2 , $R_{MS,2}$, $M_{MS,2}$, and $C_{MS,2}$ in a 1–675 Hz bandwidth, again, avoiding the anomalous 800–1000 Hz range exhibited in the sound transmission measurements and providing consistency with the TL curve



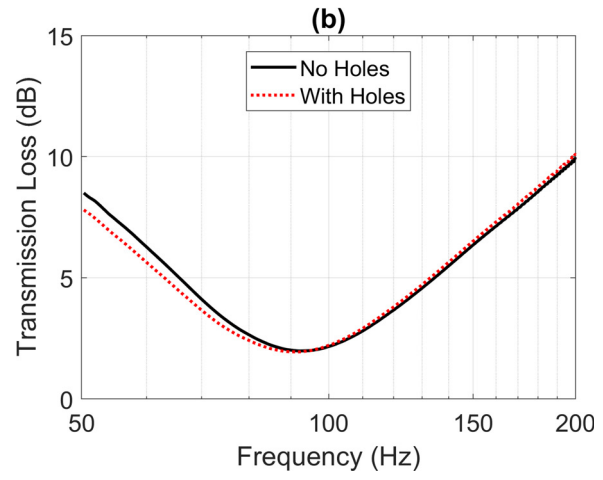


FIG. 6. Transmission loss measurements of a passive radiator using the S and P technique. (a) Known increasing masses are added for successive sound transmission measurements [arrows denote the progressive transmission loss changes starting with no added mass (dashed line) to progressively more added mass (solid lines)]. (b) Before and after holes had been cut into the spider.

fitting. Figure 7 plots the measured free-air electrical impedance magnitude with its curve fit. The agreement between the data and fit is within $1.5\,\Omega$ or 8% error over the indicated bandwidth. The authors also employed the added-mass perturbation method to compare the resulting parameters with those derived from the free-air curve-fitting method. 1,18,68

Table I reports the average parameter values extracted from these two types of electrical impedance parameter assessments for the four drivers. The parameters extracted from the added-mass and free-air electrical impedance curve-fitting methods are nearly identical, with only small differences in the values for Bl, M_{MS} , and C_{MS} . Comparing the parameters extracted from the electrical impedance curve fit to the parameters extracted from the S and P TL measurements (final curve fit) reveals that M_{MS} is 6.8% lower, C_{MS} is 10.5% higher, R_{MS} is 7.6% lower, Bl is 2.6% higher, and L_E is 21% lower for the parameters extracted from electrical impedance. Interestingly, the parameters extracted from the S and P TL using the L and A method (from the expressions given in Ref. 2) are very similar to

those from the electrical impedance curve fit, aside from the C_{MS} value.

Note that the standard deviations given in Table I, which represent deviations among the parameters extracted for the four loudspeakers tested, are not expected to be zero because some natural variation arises in the manufacturing process, but relatively lower values may give some indication of a more consistent parameter estimation technique. The standard deviations are the smallest for the S and P TL final curve fit technique among the acoustical methods, and these standard deviations are smaller than those for the electrical impedance techniques.

VI. MOVING MASS MEASUREMENT FROM DESTRUCTIVE EVALUATION

After the electrical impedance and transmission loss measurements, the authors carefully removed the moving passive radiator elements to allow analysis of their actual masses. The values followed from individual precision mass scale measurements ($\pm 0.01\,\mathrm{g}$ accuracy) of the cone assemblies, surrounds, spiders, and lead wires, which were cut from the frames and each other using a knife, scissors, and wire cutters. Figure 5(b) displays a photograph of the individual pieces from one passive radiator.

Garrett⁶⁸ showed that one-third of a spring's mass augments the effective mass of a simple mass-spring oscillator. However, as the spring of a loudspeaker suspension does not extend along a line between a fixed support point and a lumped mass, the authors decided to include the masses corresponding to the inner one-third of the annular surround and spider plus one-half of the lead wires. Because the lead wires do not provide appreciable stiffness, one-half of their lengths seemed appropriate. The expected moving mass M_{MD} then comprised the sum of the various masses.

The masses of the cone assembly, surround, spider, and lead wires for each passive radiator were averaged. The average mass of the cone assembly was 2.34 g, whereas the average combined mass of the cone assembly, entire surround, entire spider, and complete lead wires was 2.80 g.

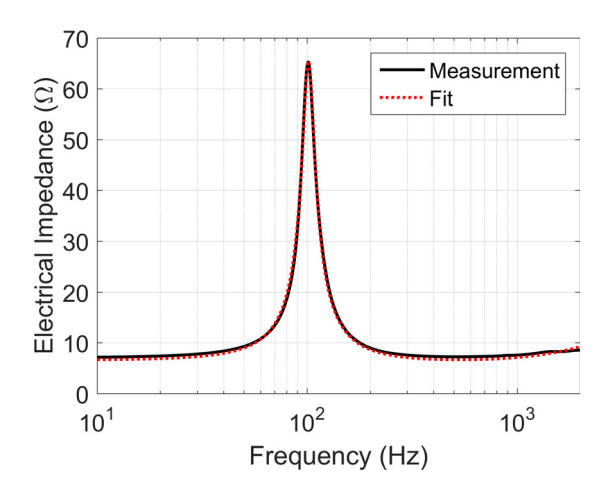


FIG. 7. A free-air electrical input impedance measurement of a loudspeaker driver with a curve fit to the data.

The average masses of the surround, spider, and lead wires were 0.25 g, 0.14 g, and 0.06 g, respectively. The expected M_{MD} involving the fractional masses of the latter three elements was 2.49 ± 0.04 g. In comparison, the average driver and passive radiator M_{MD} values obtained from the S and P sound transmission technique were 2.40 and 2.45 g, respectively. The average obtained from the free-air electrical impedance curve fit was 2.24 g. However, it is noteworthy that M_{MD} extracts directly from the sound transmission curve fitting but follows from M_{MS} and the assumed free-air fluid mass loading with the electrical impedance curve fitting. In any case, the extracted M_{MD} values should fall between 2.34 ± 0.04 and 2.80 ± 0.04 g to be physically meaningful, assuming that no less than the cone assembly moves and no more than the cone assembly plus the complete suspension and lead wires move. However, it is possible that the edges of the cone assembly do not move with the same displacement as the rest of the cone assembly, and the assumed fluid mass loading subtracted from the electrical impedance M_{MS} values is inaccurate.

Figure 8 displays the extracted average mass values with markers and error bars that extend one standard deviation below and above the average values. The dashed horizontal lines represent the 2.34 and 2.80 g physical limits of M_{MD} , and the solid horizontal line represents the expected $M_{MD} = 2.49$ g from the fractional masses obtained through destructive analysis. For the investigated drivers, it is apparent that the values obtained from electrical impedance measurements are, on average, nonphysical values less than the cone assembly's actual mass. They also present a relatively wide spread of extracted M_{MD} values for the four identical types of drivers. More realistic values might result from more careful curve fitting of the electrical impedance data. The M_{MD} values extracted using sound transmission

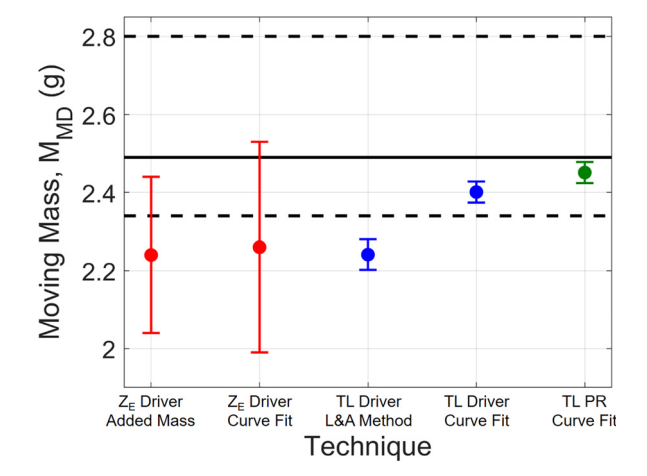


FIG. 8. Estimations of the mechanical moving mass of the cone assembly plus portions of the suspension system. The horizontal dashed lines represent the physical lower and upper bounds for the moving mass, including the cone assembly alone (lower bound) and the sum of the cone assembly plus the entire suspension system and lead wire masses (upper bound). The solid horizontal line represents the expected mass from destructive analysis. The error bars represent one standard deviation below and above the average values.



measurements and the L and A equations (L and A method) are also less than the mass of the cone assembly alone. Because the L and A equation to extract M_{MD} asymptotically approaches the actual mass, it is possible that, due to the anomaly between 800–1000 Hz, the measurement does not allow a high enough frequency TL assessment to obtain an accurate M_{MD} estimate. The M_{MD} value extracted from the TL curve fit is better and only slightly lower than the expected M_{MD} from destructive analysis (the solid horizontal line). Finally, the M_{MD} value obtained from the passive radiators using a curve fit of the TL is very close to the expected M_{MD} from destructive analysis (the solid horizontal line).

All three values for M_{MD} obtained from TL data have much less spread in their standard deviations and are about the same as the standard deviations of the direct mass measurements. Because the values extracted from TL curve fits are within the physical bounds, it is reasonable to assert that they are more reliable for the investigated drivers than the values extracted from the electrical impedance measurements or the L and A method. However, because of the limited data set used here, the analysis does not assert that some methods always yield nonphysical values while others produce superior values. The primary aim is to present methods and results from plane wave tubes measurements for experimental driver and passive radiator parameter extractions and then compare the associated M_{MD} values to results from direct physical mass measurements.

VII. CONCLUSIONS

This paper has explored the experimental feasibility of sound transmission measurements of loudspeaker drivers and passive radiators (DUTs) that do not rely on ideal anechoic terminations for parameter extractions, as assumed experimentally in the past.³⁹ The investigation has affirmed that normal-incidence sound transmission measurements can extract moving-coil loudspeaker driver parameters comparable to those derived from electrical impedance measurements. As suggested previously² and shown here experimentally for the first time, a plane wave tube system can readily characterize passive radiators and their changes, electrical impedance techniques Expressions developed by L and A² and curve-fitting optimization methods produced acoustically derived parameters from sound transmission measurements. Curve-fitting methods produced parameters from electrical impedance measurements. Assessing driver parameters from electrical impedance measurements is often easier and faster. The work considered the accuracy and robustness of each type of assessment for the drivers tested, but the purpose was not to draw firm general conclusions. One primary consideration in using plane wave tubes to measure sound transmission through DUTs is that their cross-sectional dimensions dictate the upper-frequency limits on one-dimensional sound propagation. However, the measurement method scales such that larger or smaller tube diameters allow approximate

piston-band assessments of larger or smaller DUTs, respectively.

The two-load transmission loss measurement technique outlined by S and P⁵³ allows the extraction of sound transmission through DUTs with imperfect downstream anechoic terminations described by L and A.2 As a drawback, the technique requires two sound transmission measurements for each DUT. Nevertheless, the two measurements allow accurate characterizations of the mechanical parameters of passive radiators and any changes made to them. They also provide loudspeaker drivers' mechanical and electrical parameters through open- and closed-circuit terminal conditions. A single electrical impedance measurement and subsequent curve fitting may produce the same parameters. However, the latter may include inherent contamination of the extracted mechanical parameters, e.g., cause by a position-dependent force factor Bl_{1}^{22} and they cannot directly characterize passive radiators.

Electrical impedance measurements and the L and A TL formulations produced nonphysical average values for the estimated moving mass of a cone assembly and suspension system with the drivers tested here. In contrast, a curve fitting of the TL measurements yielded physically tenable results. Because the investigation involved only a limited number of drivers, one may not generally conclude, without further investigation, that these techniques will produce similar results when applied to other drivers. The average moving mass value of passive radiators from TL curve fitting was only 1.6% less than the average directly measured mass after destructive disassembly. The acoustic mass loading of a driver with its motor assembly in place probably differs from that of a corresponding passive radiator with the motor assembly removed. Furthermore, the assumption that the fluid loading of a driver or passive radiator is the same as that observed by an unbaffled vibrating piston in free space may be unreliable. Sound transmission measurements of a passive radiator with known masses added successively to the cone produced only a 1.4% average error. The measurements also detected modifications to the passive radiator suspension compliance.

A deeper analysis of various factors influencing the reported experimental outcomes is beyond the scope of the present work. These factors could include background noise, specific termination choices for sound transmission measurements, measurement and curve-fitting bandwidths, the use of a simplified blocked electrical impedance model for the voice coil, and nonlinear effects. Future work could address these effects, various sources of error, accuracy limitations, and other matters to enhance the practicality of sound transmission measurements of loudspeaker drivers and passive radiators.

ACKNOWLEDGMENTS

The authors thank the Brigham Young University (BYU) College of Computational, Mathematical, and Physical Sciences for supporting this research.



AUTHOR DECLARATIONS Conflict of Interest

The authors have no conflicts of interest to disclose.

DATA AVAILABILITY

The data that support the findings of this study are available from the corresponding author upon reasonable request.

- ¹J. D'Appolito, *Testing Loudspeakers* (Audio Amateur, Peterborough, NH, 1998), pp. 9–36.
- ²T. W. Leishman and B. E. Anderson, "Evaluation of moving-coil loud-speaker and passive radiator parameters using normal-incidence transmission loss measurements: Theoretical developments," J. Acoust. Soc. Am. **134**(1), 223–236 (2013).
- ³A. N. Thiele, "Loudspeakers in vented boxes: Parts I and II," Proc. IREE Aust. **22**, 487–508 (1961) [reprinted in J. Audio Eng. Soc. **19** 382–392, 471–483 (1971)], available at https://aes2.org/publications/elibrary-page/?id=2173.
- ⁴J. R. Ashley and M. D. Swan, "Improved measurement of loudspeaker parameters," in *40th Convention of the Audio Engineering Society*, Los Angeles, CA (April 27–30, 1971), preprint 803.
- ⁵R. H. Small, "Closed-box loudspeaker systems, Part I: Analysis," J. Audio Eng. Soc. **20**, 798–808 (1972), available at https://aes2.org/publications/elibrary-page/?id=2022.
- ⁶R. H. Small, "Closed-box loudspeaker systems, Part II: Synthesis," J. Audio Eng. Soc. **21**, 11–18 (1973), available at https://aes2.org/publications/elibrary-page/?id=2011.
- ⁷W. J. J. Hoge, "The measurement of loudspeaker driver parameters," in *58th Convention of the Audio Engineering Society*, New York (November 4–7, 1977), preprint 1287.
- ⁸W. Leach, R. Schafer, and T. Barnwell, "Time domain measurement of loudspeaker driver parameters," IEEE Trans. Acoust., Speech, Signal Proc. ASSP-27, 322–325 (1979).
- ⁹J. R. Ashley, "Home computer aided measurement of loudspeaker driver parameters," in *Proceedings—IMTC'85*, *IEEE*, *Instrumentation and Measurement Technology Conference*, Tampa, FL (March 20–22, 1985), pp. 269–273.
- ¹⁰R. C. Cabot, "Automated measurements of loudspeaker small signal parameters," in 81st Convention of the Audio Engineering Society, Los Angeles, CA (November 12–16, 1986), preprint 2402.
- ¹¹C. J. Struck, "Determination of the Thiele-Small parameters using twochannel FFT analysis," in 82nd Convention of the Audio Engineering Society, London, UK (March 1, 1987), preprint 2446.
- ¹²J. R. Ashley, "Simple measurements for home loudspeaker systems," in Proceedings—IMTC '88, IEEE Instrumentation and Measurement Technology Conference, San Diego, CA (April 20–22, 1988), pp. 341–344.
- ¹³A. N. Thiele, "Measurement of the Thiele/Small parameters of tweeters," J. Electr. Electron. Eng., Aust. 9, 186–199 (1989).
- ¹⁴R. Gomez-Meda, "Measurement of the Thiele-Small parameters for a given loudspeaker without using a box," in *91st Convention of the Audio Engineering Society*, New York (October 4–8, 1991), preprint 3162.
- ¹⁵E. Geddes and A. Phillips, "Efficient loudspeaker linear and nonlinear parameter estimation," in 91st Convention of the Audio Engineering Society, New York (October 4–8, 1991), preprint 3164.
- ¹⁶H. Blind, A. Phillips, and E. Geddes, "Efficient loudspeaker parameter estimation—An extension," in 93rd Convention of the Audio Engineering Society, San Francisco, CA (October 1–4, 1992), preprint 3430.
- ¹⁷A. P. Berkhoff, "Impedance analysis of subwoofer systems," J. Audio Eng. Soc. 42, 4–13 (1994).
- ¹⁸W. M. Leach, *Introduction to Electroacoustics and Audio Amplifier Design*, 2nd ed. (Kendall/Hunt, Dubuque, IA, 2001), p. 301–307.
- ¹⁹R. Ravaud, G. Lemarquand, V. Lemarquand, and T. Roussel, "Ranking of the nonlinearities of electrodynamic loudspeakers," J. Arch. Acoust. 35(1), 49–66 (2010).
- ²⁰J. Christophorou, "Low-frequency loudspeaker measurements with an accelerometer," J. Audio Eng. Soc. 28, 809–816 (1980), available at https://aes2.org/publications/elibrary-page/?id=3945.

- ²¹J. N. Moreno, "Measurement of loudspeaker parameters using a laser velocity transducer and two-channel FFT analysis," J. Audio Eng. Soc. 39, 243–249 (1991), available at https://aes2.org/publications/elibrary-page/?id=5988.
- ²²D. Clark, "Precision measurement of loudspeaker parameters," J. Audio Eng. Soc. 45, 129–141 (1997), available at https://aes2.org/publications/ elibrary-page/?id=7867.
- ²³W. Klippel, "Measurement of large-signal parameters of electrodynamic transducer," in *107th Convention of the Audio Engineering Society*, New York (September 24–27, 1999), preprint 1999.
- ²⁴E. R. Geddes, "Method for determining transducer linear operational parameters," U.S. patent 6,269,318 (July 31, 2001).
- ²⁵W. Klippel, "Dynamic measurement of loudspeaker suspension parts," J. Audio. Eng. Soc. **56**, 453–459 (2007), available at https://aes2.org/publications/elibrary-page/?id=14167.
- ²⁶M. R. Bai and C.-M. Huang, "Expert diagnostic system for moving-coil loudspeakers using nonlinear modeling," J. Acoust. Soc. Am. **125**(2), 819–830 (2009).
- ²⁷Y.-T. Tsai, C.-C. Wang, and J. H. Huang, "An inverse method for estimating the electromechanical parameters of moving-coil loudspeakers," J. Acoust. Soc. Am. **134**(5), 3594–3604 (2013).
- ²⁸X. Kong, X. Zeng, and K. Han, "Dynamical measurements on viscoelastic behaviors of spiders in electro-dynamic loudspeakers," J. Appl. Acoust. 104, 67–75 (2016).
- ²⁹Y.-C. Jian, Y.-T. Tsai, and S. J. Pawar, "Parameter optimization method for identifying the optimal nonlinear parameters of a miniature transducer with a metal membrane," J. Appl. Sci. 8(12), 2647 (2018).
- ³⁰V. K. Jain, W. M. Leach, and R. W. Schafer, "Signal processing technique for measurement of vented-box loudspeaker system parameters," in *Proceedings—ICASSP '82, IEEE, Acoustics, Speech, and Signal Processing Conference*, Paris, France (May 3–5, 1982), pp. 1428–1431.
- ³¹M. Ureda, "Determination of Thiele-Small parameters of a loudspeaker using nonlinear goal programming," in 72nd Convention of the Audio Engineering Society, Anaheim, CA (October 23–27, 1982), preprint 1953.
- ³²V. Jain, W. Leach, and R. W. Schafer, "Time-domain measurement of vented-box loudspeaker system parameters," IEEE Trans. Acoust., Speech, Signal Proc. ASSP-31, 1–8 (1983).
- ³³Y. Nomura, T. Ai, and K. Fukuda, "Estimation method of direct-radiator loudspeaker system parameters in low-frequency range by nonlinear optimization rechnique," Electron. Commun. Jpn., Part 1 69, 18–27 (1986) [translated from Denshi Tsushin Gakkai Ronbunshi 68-A, 504–511 (1985)].
- ³⁴M. H. Knudsen, J. G. Jensen, V. Julskjaer, and P. Rubak, "Determination of loudspeaker driver parameters using a system identification technique," J. Audio Eng. Soc. 37, 700–708 (1989), available at https://aes2.org/ publications/elibrary-page/?id=6072.
- ³⁵W. Waldman, "Nonlinear least squares estimation of Thiele-Small parameters from impedance measurements," in *94th Convention of the Audio Engineering Society*, Berlin, Germany (March 1, 1993), preprint 3511.
- String Society, Berlin, Germany (March 1, 1995), preprint 3311.
 K.-P. Kong, F. Agerkvist, and X.-W. Zeng, "Modeling of lossy inductance in moving-coil loudspeakers," Acta Acust. 101, 650–656 (2015).
- ³⁷J. Borwick, *Loudspeaker and Headphone Handbook*, 3rd ed. (Focal, Woburn, MA, 2001), p. 306.
- ³⁸AES19-1992: ALMA TM-100, AES—ALMA Standard Test Method for Audio Engineering—Measurement of the Lowest Resonance Frequency of Loudspeaker Cones (Audio Engineering Society, New York, 1992) [withdrawn 2003].
- ³⁹B. E. Anderson and T. W. Leishman, "An acoustical measurement method for the derivation of loudspeaker parameters," in 115th Convention of the Audio Engineering Society, New York (October 10–13, 2003), p. 5865.
- ⁴⁰W. Klippel, "Tutorial: Loudspeaker nonlinearities—Causes, parameters, symptoms," J. Audio. Eng. Soc. 54, 907–939 (2006), available at https://aes2.org/publications/elibrary-page/?id=13881.
- ⁴¹J. Y. Chung and D. A. Blaser, "Transfer function method of measuring induct acoustic properties. I. Theory," J. Acoust. Soc. Am. 68, 907–913 (1980).
- ⁴²J. Y. Chung and D. A. Blaser, "Transfer function method of measuring induct acoustic properties. II. Experiment," J. Acoust. Soc. Am. 68, 914–921 (1980).
- ⁴³AES 1id-1991: AES Information Document—Plane-Wave Tubes: Design and Practice (Audio Engineering Society, New York, 1991).

https://doi.org/10.1121/10.0039708



- ⁴⁴A. F. Seybert and D. F. Ross, "Experimental determination of acoustic properties using a two-microphone random-excitation technique," J. Acoust. Soc. Am. 61, 1362–1370 (1977).
- ⁴⁵S. Riggs and E. Geddes, "A two microphone technique for the measurement of acoustic waveguide impedance," in 87th Convention of the Audio Engineering Society, New York (October 18–21, 1989), preprint 2878.
- ⁴⁶ISO 10534-1:1996 and 2:1998: "Acoustics—Determination of sound absorption coefficient and impedance in impedance tubes— Parts 1 and 2" (International Organization for Standardization, Geneva, Switzerland, 1996 and 1998).
- ⁴⁷B. F. G. Katz, "Method to resolve microphone and sample location errors in the two-microphone duct measurement method," J. Acoust. Soc. Am. 108, 2231–2237 (2000).
- ⁴⁸M. R. Bai, Y.-Y. Lo, and Y. S. Chen, "Impedance measurement techniques for one-port and two-port networks," J. Acoust. Soc. Am. 138, 2279–2290 (2015).
- ⁴⁹Z. Wei, H. Hou, N. Gao, Y. Huang, and J. Yang, "Normal incidence sound transmission loss evaluation with a general upstream tube wave decomposition formula," J. Acoust. Soc. Am. 144(4), 2344–2353 (2018).
- ⁵⁰T. Y. Lung and A. G. Doige, "A time-averaging transient testing method for acoustic properties of piping systems and mufflers with flow," J. Acoust. Soc. Am. 73, 867–876 (1983).
- ⁵¹B. H. Song and J. S. Bolton, "A transfer matrix approach for estimating the characteristic impedance and wave number of limp and rigid porous materials," J. Acoust. Soc. Am. 107, 1131–1152 (2000).
- ⁵²J. S. Bolton, T. Yoo, and O. Olivieri, "Measurement of normal incidence transmission loss and other acoustical properties of materials placed in a standing wave tube," Bruel Kjaer, Tech. Rev. 1, 1–44 (2007).
- ⁵³Y. Salissou and R. Panneton, "A general wave decomposition formula for the measurement of normal incidence sound transmission loss in impedance tube," J. Acoust. Soc. Am. 125, 2083–2090 (2009).
- ⁵⁴L. E. Kinsler, A. R. Frey, A. B. Coppens, and J. V. Sanders, Fundamentals of Acoustics, 4th ed. (Wiley, New York, 2000), pp. 212– 214, 228–234, and Appendix A10.
- ⁵⁵A. D. Pierce, Acoustics, An Introduction to Its Physical Principles and Applications, 3rd ed. (Springer and ASA, Cham, Switzerland, 2019), pp. 223–224 and 364–365.
- ⁵⁶J. D. Sagers, T. W. Leishman, and J. D. Blotter, "Active sound transmission control of a double-panel module using decoupled analog feedback control: Experimental results," J. Acoust. Soc. Am. 128(5), 2807–2816 (2010)

- ⁵⁷IEC 60268-22: Sound System Equipment—Part 22: Electrical and Mechanical Measurements on Transducers (International Electrotechnical Commission, Geneva, Switzerland, 2020).
- ⁵⁸W. Klippel and J. Schlecter, "Dynamic measurement of transducer effective radiation area," J. Audio Eng. Soc. **59**, 44–52 (2011), available at https://aes2.org/publications/elibrary-page/?id=15775.
- ⁵⁹J. D. Sagers, T. W. Leishman, and J. D. Blotter, "An extended lumpedelement model and parameter estimation technique to predict loudspeaker responses with possible surround-dip effects," J. Acoust. Soc. Am. 134(5), 3580–3593 (2013).
- ⁶⁰ASTM E1050-24: Standard Test Method for Impedance and Absorption of Acoustical Materials Using a Tube, Two Microphones and a Digital Frequency Analysis System (American Society for Testing and Materials, Philadelphia, PA, 2024).
- ⁶¹ASTM E2611-24: Standard Test Method for Normal Incidence Determination of Porous Material Acoustical Properties Based on the Transfer Matrix Method (American Society for Testing and Materials, Philadelphia, PA, 2024).
- ⁶²H. Bodén and M. Åbom, "Influence of errors on the two-microphone method for measuring acoustic properties in ducts," J. Acoust. Soc. Am. 79, 541–549 (1986).
- ⁶³S. M. Young, B. E. Anderson, R. C. Davis, R. R. Vanfleet, and N. B. Morrill, "Sound transmission measurements through porous screens," Proc. Mtgs. Acoust. 26, 045003 (2017).
- ⁶⁴Z. Chen and N. Xiang, "Bayesian estimation of dissipation and sound speed in tube measurements using a transfer-function model," J. Acoust. Soc. Am. 155, 2646–2658 (2024).
- ⁶⁵K. Thorborg and A. D. Unruh, "Electrical equivalent circuit model for dynamic moving-coil transducers incorporating a semi-inductor," J. Audio Eng. Soc. 56(9), 696–709 (2008), available at https://aes2.org/ publications/elibrary-page/?id=14633.
- ⁶⁶J. C. Lagarias, J. A. Reeds, M. H. Wright, and P. E. Wright, "Convergence properties of the Nelder–Mead simplex method in low dimensions," SIAM J. Optim. 9(1), 112–147 (1998).
- ⁶⁷B. E. Anderson, "Derivation of moving-coil loudspeaker parameters using plane wave tube techniques," Master's thesis, Brigham Young University (2003), available at https://scholarsarchive.byu.edu/etd/17 (Last viewed August 14, 2025).
- ⁶⁸S. L. Garrett, *Understanding Acoustics*, 2nd ed. (ASA and Springer, Cham, Switzerland, 2017), pp. 68–69 and 95–98.